Multiple-polariton scattering in a semiconductor microcavity



2004 J. Phys.: Condens. Matter 16 S3653

(http://iopscience.iop.org/0953-8984/16/35/007)

INSTITUTE OF PHYSICS PUBLISHING JOURNAL OF PHYSICS: CONDENSED MATTER

J. Phys.: Condens. Matter **16** (2004) S3653–S3664 PII: S0953-8984(04)83317-4

# Multiple-polariton scattering in a semiconductor microcavity

**N A Gippius and S G Tikhodeev**[1]

General Physics Institute RAS, Vavilova 38, Moscow 119991, Russia

E-mail: tikh@gpi.ru

Received 6 July 2004
Published 20 August 2004
Online at stacks.iop.org/JPhysCM/16/S3653
doi:10.1088/0953-8984/16/35/007

**Abstract**

Recently an unusual behaviour of the polariton–polariton scattering in a semiconductor microcavity (MC) under a strong continuous resonant excitation near the lower polariton branch has been observed (Kulakovskii *et al* 2001 *Nanotechnology* **12** 475). The maxima of the scattered photoluminescence signal above the threshold of parametric scattering does not shift along the microcavity lower polariton branch with change of the pump detuning or angle of incidence but is always directed approximately perpendicular to the MC plane. We discuss theoretically a possible explanation of such behaviour via a competition between two instabilities in the polariton–polariton scattering, stimulated polariton–polariton scattering *and* bistability of the pumped polariton mode response.

(Some figures in this article are in colour only in the electronic version)

## 1. Introduction

Since the pioneering work by Weisbuch *et al* [1] a lot of exciting physics has been established in the system of quasi-two-dimensional (2D) polaritons in a semiconductor microcavity [2]. Recently, a very effective polariton–polariton scattering under the resonant excitation close to the inflection point of the lower polariton (LP) branch has been observed under pulse [3] and continuous [4–6] excitation. Giant parametric gains have been found [3] and explained theoretically [7] as a MC polariton parametric amplifier, with threshold dependence of the coherent gain due to renormalized (blue-shifted) polariton four-wave mixing. A strong polarization dependence of the stimulated scattering [8] proves the importance of the bosonic nature of MC polaritons. A strong redistribution of the polariton parametric luminescence has been established under continuous excitation near the inflection point [5, 6]. Theoretically, the

[1] Author to whom any correspondence should be addressed.

  

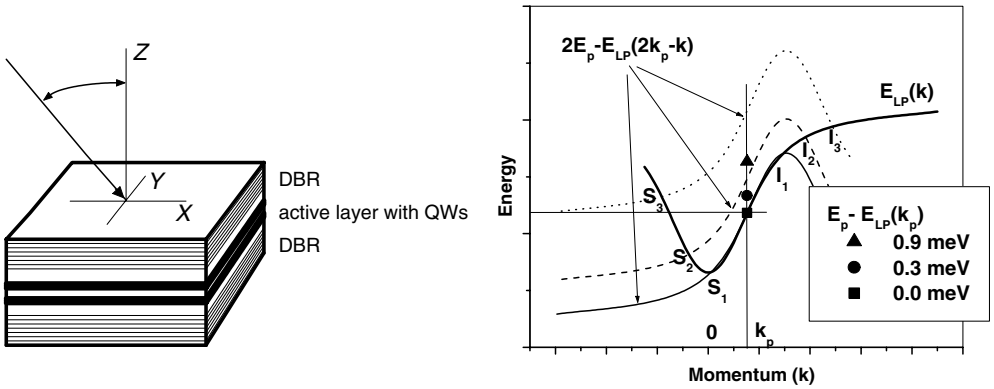


**Figure 1.** Left panel: a schematic representation of light scattering from a planar semiconductor microcavity, composed of a $\lambda$ or $(3/2)\lambda$ cavity with active quantum wells (QWs), sandwiched between two distributed Bragg reflectors (DBR). Right panel: a schematic representation of the polariton–polariton scattering, equations (1), (2), at low pump energies. The thick solid curve is the LP polariton branch $E_{\mathrm{LP}}(\mathbf{k})$. The thin lines are the conjugated idler branches $2E_{\mathrm{p}} - E_{\mathrm{LP}}(2\mathbf{k}_{\mathrm{p}} - \mathbf{k})$ at resonant pump energies with increasing energy detuning $E_{\mathrm{p}} - E_{\mathrm{LP}}(\mathbf{k}_{\mathrm{p}})$ (symbols). It is shown that the signal (S) and idler (I) have to shift along the LP branch with increase of the detuning.

effect was explained by the renormalization of the LP polariton spectra due to the parametric coupling [7, 9, 10]. The spectra and occupation number transformations become especially drastic above the threshold of parametric scattering under cw excitation, when multiply scattered polariton macro-occupied modes can develop [11]. The effect of polariton parametric amplification was shown to survive at high temperatures up to 120 K in GaAlAs-based MC and up to 220 K in CdTe-based microcavities [12].

The polariton–polariton scattering in a microcavity (see a scheme in figure 1) occurs with energy and lateral momentum conservation and results in two sharp emission peaks on the LP branch $E_{\mathrm{LP}}(\mathbf{k})$, the 'signal' at $\mathbf{k}_{\mathrm{s}}$ and 'idler' at $\mathbf{k}_{\mathrm{i}}$:

$$\mathbf{k}_{\mathrm{s}} + \mathbf{k}_{\mathrm{i}} = 2\mathbf{k}_{\mathrm{p}}, \tag{1}$$

$$E_{\mathrm{LP}}(\mathbf{k}_{\mathrm{s}}) + E_{\mathrm{LP}}(\mathbf{k}_{\mathrm{i}}) = 2E_{\mathrm{p}}, \tag{2}$$

where $\mathbf{k}_{\mathrm{p}}$ and $E_{\mathrm{p}}$ are the pump photon in-plane momentum and energy. The striking transformations of the polariton parametric luminescence with increase of the intensity of the resonant cw coherent excitation [4–6, 8, 11] have been investigated experimentally mostly in the case of specific pump conditions known as *magic angle* excitation. This is when the pump momentum is close to the LP branch inflection point, and the scattered polaritons have $k_{\mathrm{s}} \approx 0$, $k_{\mathrm{i}} \approx 2k_{\mathrm{p}}$; see figure 1.

What happens if, however, the pump is set away from the magic angle conditions? At low pump energies, when only one (pumped) polariton mode is macroscopically occupied, the signal and idler have to shift along the LP dispersion branch with increase of the detuning, as illustrated by the graphical solutions of equations (1), (2) in figure 1. In a naive understanding, new macro-occupied modes have to develop above the parametric scattering threshold in the regions of such signal and idler branch intersections.

However, under stationary excitation conditions, and for high enough pump intensity, the behaviour of the scattered polaritons appears to be much more complicated than that according to this simple picture. It has been demonstrated [14] and confirmed very recently [15] that in the case of stationary excitation, and for high pump energies above the threshold of parametric scattering, the signal and idler do not shift along the LP dispersion curve with the growth of

detuning, but peak around $k_s \approx 0$, $k_i \approx 2k_p$, i.e. as for excitation near the inflection point. In what follows, we discuss a possible explanation of this unexpected behaviour in the polariton–polariton scattering [16, 17].

## 2. The one-dimensional model of polariton–polariton scattering: the parametric scattering threshold versus the pumped exciton bistability

In order to model the parametric polariton–polariton scattering theoretically, we have solved numerically [16, 17] a system of coupled equations for $\mathcal{E}_{QW}$, the electric field inside the microcavity (on the QW), and $\mathcal{P}(k, t)$, the averaged exciton polarization over the QW thickness, given by

$$\left[\mathrm{i}\frac{\mathrm{d}}{\mathrm{d}t} - E_C(k)\right]\mathcal{E}_{QW}(k,t) = \alpha(k)\mathcal{E}_{ext}(k,t) + \beta(k)\mathcal{P}(k,t), \tag{3}$$

$$\left[\mathrm{i}\frac{\mathrm{d}}{\mathrm{d}t} - E_X\right]\mathcal{P}(k,t) = A\mathcal{E}_{QW}(k,t) + F\sum_{q,q'}\mathcal{P}(q,t)\mathcal{P}(q',t)\mathcal{P}^*(q+q'-k,t) + \xi(t). \tag{4}$$

Here $\mathcal{E}_{ext} = \mathcal{E}(t)\exp(-\mathrm{i}E_p t)\delta(k - k_p)$ is the electric field of the pump light far from the MC, which is assumed to be a macro-occupied photonic mode with fixed energy $E_p$, wavenumber $k_p = E_p \sin\vartheta/c$ (where $\vartheta$ is the angle of pump incidence) and amplitude slowly changing with time $\mathcal{E}(t)$. $E_C$ and $E_X$ are the resonant frequency of the empty MC and the free exciton energy in an isolated QW, respectively, $F$ is the exciton–exciton coupling constant, $A$ is the exciton polarizability, $\xi(k, t)$ is the stochastic Langevin force, $\langle\xi(k,t)\rangle = 0$ and $\langle\xi(k,t)\xi(k',t')\rangle = \Xi\delta(k-k')\delta(t-t')$. The MC response constants $\alpha$ and $\beta$ can be found through the resonant approximation for the MC scattering matrix at $\omega = E_C(k)$. The energy is measured in millielectronvolts, and the units of polarization and electric field are such that $F = 1$. In order to simplify the situation, only a one-dimensional (1D) model is considered, when all scattered polariton momenta are aligned along the direction of intersection between the pump plane of incidence and the MC plane. Another simplification is omitting the so-called saturation term [7] (due to the fermion compound nature of the exciton). In the next section we will discuss the physical consequences of the two-dimensionality of the polariton–polariton scattering, and accounting for the exciton saturation.

Equation (3) is the Maxwell equation with exciton polarization, written in a resonant scalar approximation. This means that we neglect the interaction between $\sigma^{\pm}$-polarized polaritons. Equation (4) is the inhomogeneous nonlinear Schrödinger equation for the exciton polarization with two sources: coherent external pumping and stochastic Langevin noise. The latter allows us to model the quantum fluctuations of the scattered signals using quasiclassical equations (3) and (4).

Numerical solutions of equations (3) and (4) demonstrate a sharp transition from a regular behaviour at lower pump intensities to a strongly fluctuating behaviour above an abrupt threshold. Typical solutions are illustrated in figures 2 and 3. In figure 2 the integrated angular distribution of the scattered light (over the duration of the 1000 ps pump pulse; the dash–dotted curve in the inset in figure 3) is depicted below (left panel) and above (right panel) the transition.

The solution below the threshold (left panel in figure 2) coincides with that in [9, 10]—the signal and idler are peaked around the intersections of the renormalized signal and idler LP dispersion branches. If the pump detuning is positive (pump energy above the LP branch), the signal and idler peaks are at $k_s < 0$ ($\vartheta_s < 0$), $k_i > 2k_p$, in agreement with the simple picture in figure 1, but accounting for the LP branch blue-shift with increase of the pump energy.

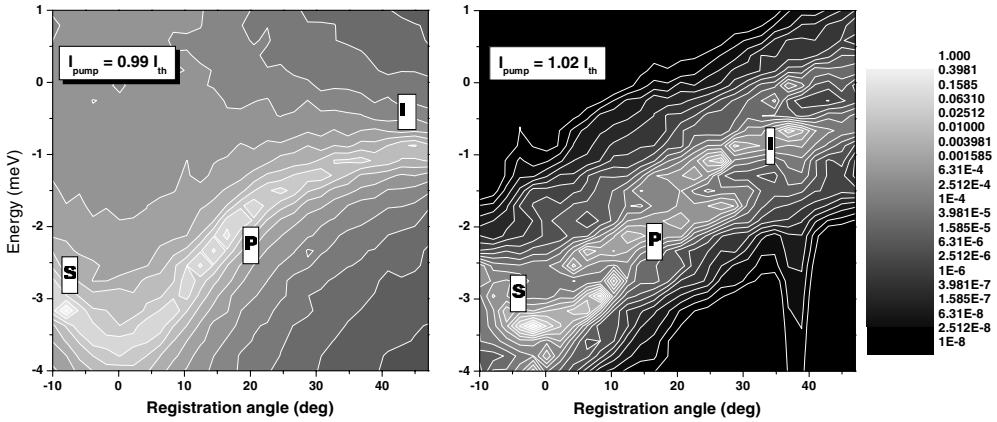


**Figure 2.** The calculated scattered light intensity distribution below (left panel) and above (right panel) the threshold. The signal, pump and idler are marked with labels S, P and I, respectively. Energy detuning is measured from the empty cavity resonance at $k = 0$ and the exciton energy in the quantum well is assumed to be 1 meV below. The scattered intensity in both panels is normalized and shown on a logarithmic greyscale. Note that the range of intensity modulation in the left panel (below the threshold) is ∼4 orders of magnitude lower than that in the right panel (above the threshold).

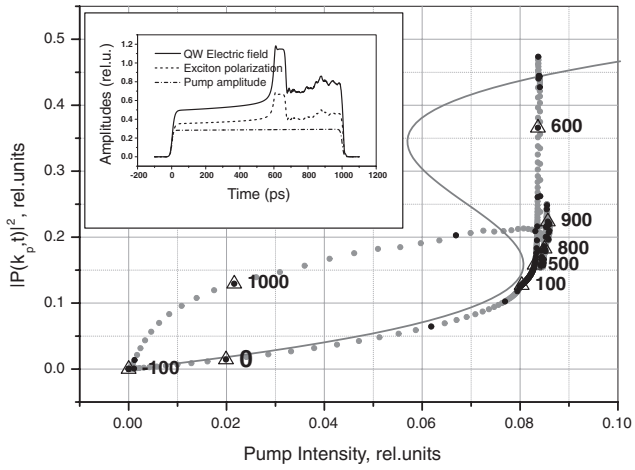


**Figure 3.** Exciton polarization versus pump intensity during the excitation pulse. The time delay between grey, black and triangled dots is 1, 10 and 100 ps, respectively; the triangles are labelled with the time in picoseconds. The solid S-shaped curve is the solution of equation (7) for a stationary pump amplitude. The inset shows the time dependences of the input excitation pulse (dash–dotted line), the calculated exciton polarization (dotted curve) and the QW electric field (solid curve).

Above the threshold a qualitatively different behaviour is seen (right panel in figure 2). The scattered signal undergoes an abrupt jump from the resonant momentum $k_s < 0$ towards the normal direction $k_s \approx 0$ and its intensity in the normal direction becomes significantly stronger than just before the threshold. Note that the difference in pump intensity between the right and left panels in figure 2 is only ≈3%. The averaged intensity of the scattered noise above the transition increases by several orders of magnitude (note the logarithmic greyscale in figure 2).

Figure 3 explains the time kinetics of the scattering above the threshold pump intensity. The shape of the excitation pulse $\mathcal{E}_{\rm ext}^2$ (the dash–dotted line in the inset in figure 3) was chosen in such a way that the threshold intensity is approached slowly during the pulse duration. Actually two sharp transitions take place (at $t \approx 600$ and 700 ps). Both transitions are characterized by jumps of the driven mode amplitude $\mathcal{P}_0$ and the electric field on the quantum well $\mathcal{E}_0$; see the solid and dotted curves, respectively, in figure 3, inset. From the kinetics of the driven exciton shown by dots in figure 3, it can be easily seen that the first transition at $t \approx 600$ ps is actually not the parametric scattering instability. It is rather the bistability of the driven nonlinear oscillator response to the external force.

In order to understand the sharp transitions, which are characteristic for the numerical solutions of equations (3) and (4), we have to investigate the stability of the solutions in the case of a stationary external field $\mathcal{E}_{\rm ext}(t) =$ constant with only one macroscopically filled mode, i.e., of the form

$$\mathcal{P}(k,t) = \tilde{\mathcal{P}}(k,t) + \delta_{k,k_{\rm p}}\mathcal{P}_0 {\rm e}^{-{\rm i}E_{\rm p}t} \tag{5}$$

and

$$\mathcal{E}_{\rm QW}(k,t) = \tilde{\mathcal{E}}(k,t) + \delta_{k,k_{\rm p}}\mathcal{E}_0 {\rm e}^{-{\rm i}E_{\rm p}t}. \tag{6}$$

Here $\tilde{\mathcal{P}}$ and $\tilde{\mathcal{E}}$ are assumed to be small deviations from the solution with one macro-occupied mode, $|\tilde{\mathcal{P}}/\mathcal{P}_0|, |\tilde{\mathcal{E}}/\mathcal{E}_0| \ll 1$. Such a stability analysis corresponds well to our physical situation when the initial populations of all exciton modes are small compared to that of the pumped mode.

In zero order over $\tilde{\mathcal{P}}$ and $\tilde{\mathcal{E}}$ we get the following cubic equation for the amplitude of the driven mode $\mathcal{P}_0$:

$$(\Delta_{\rm PC}\Delta_{\rm PX} - A\beta)\,\mathcal{P}_0 - \Delta_{\rm PC}F|\mathcal{P}_0|^2\mathcal{P}_0 = A\alpha\mathcal{E}_{\rm ext}, \tag{7}$$

where $\Delta_{\rm PC} = E_{\rm p} - E_{\rm C}(k_{\rm p})$, $\Delta_{\rm PX} = E_{\rm p} - E_{\rm X}(k_{\rm p})$.

The calculated solution of equation (7) (with the same input parameters as in figure 2) is an S-shaped curve shown as a solid curve in figure 3 and, additionally, in figure 4. The S-shape is usual in the theory of nonlinear cavities (see, e.g., [18–20]). Actually, this fact is well known in the theory of nonlinear driven oscillators since at least the pioneering work of Duffing [21] (see, e.g., reviews [22, 23]); it brings a *bistability* into the behaviour of the MC polaritons. The influence of the bistability was not analysed in the existing theories of the MC polariton scattering [7, 9–11, 13]. Only recently has the bistability been found experimentally in MC polaritons, under resonant excitation into the bottom of the LP branch [24].

It can be easily seen that the first instability of the polariton scattering at $t \approx 600$ ps is actually the jump of the driven nonlinear oscillator from the lower S-curve branch (becoming unstable with increase of the external pump) to the upper S-curve branch. In the empty cavity with quadratic dispersion, the upper S′-curve branch is usually stable [18, 19]. However, in the case of polariton–polariton scattering in a MC we see that this branch may become unstable too (see a transition at $t \approx 700$ ps in figure 3).

In order to understand the physical reason for that, we have to analyse the stability conditions, linearizing equations (3) and (4) over small deviations, and solve the linear eigenproblem for parametrically coupled deviation amplitudes of the signal $\tilde{\mathcal{E}}(k,t) = \tilde{\mathcal{E}}(k)\exp(-{\rm i}\omega t)$, $\tilde{\mathcal{P}}(k,t) = \tilde{\mathcal{P}}(k)\exp(-{\rm i}\omega t)$ and idler $\tilde{\mathcal{E}}^*(\bar{k},t)\exp(-2{\rm i}E_{\rm p}t) = \bar{\tilde{\mathcal{E}}}(\bar{k})\exp(-{\rm i}\omega t)$, $\tilde{\mathcal{P}}^*(\bar{k},t)\exp(-2{\rm i}E_{\rm p}t) = \bar{\tilde{\mathcal{P}}}(\bar{k})\exp(-{\rm i}\omega t)$ (where $\bar{k} = 2k_{\rm p} - k$):

$$\omega\begin{pmatrix}\tilde{\mathcal{E}}(k)\\ \tilde{\mathcal{P}}(k)\\ \bar{\tilde{\mathcal{E}}}(\bar{k})\\ \bar{\tilde{\mathcal{P}}}(\bar{k})\end{pmatrix} = \hat{H}_{\rm eff}\begin{pmatrix}\tilde{\mathcal{E}}(k)\\ \tilde{\mathcal{P}}(k)\\ \bar{\tilde{\mathcal{E}}}(\bar{k})\\ \bar{\tilde{\mathcal{P}}}(\bar{k})\end{pmatrix}. \tag{8}$$

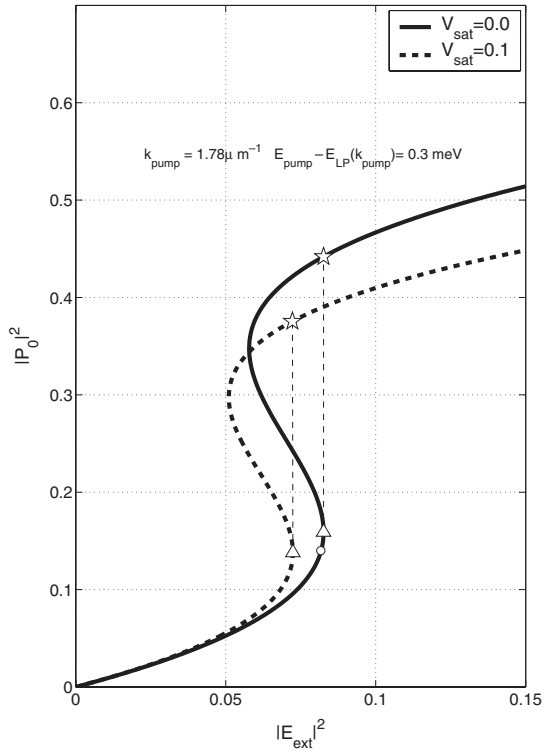


**Figure 4.** S-shaped dependences of the amplitude of the driven nonlinear exciton versus external electric field, calculated without saturation (solid curve, as in figure 3) and with saturation, $V_{\rm sat} = 0.1$ (dashed curve). An empty circle on the solid S-curve shows the threshold of the parametric instability, where the renormalized spectra in figure 5 are calculated. Upward pointing triangles are the ends of the lower stable S-curve branches; the renormalized spectra at these points are shown in figures 7(a), (b) and 8(a), (b). Stars mark the pumped exciton states on the upper stable S-curve branches; the respective renormalized spectra are shown in figures 6, 7(c), (d), and 8(c), (d).

Here the effective energy matrix $\hat{H}_{\rm eff}$ is

$$\begin{pmatrix} E_{\rm C}(k) & \beta & 0 & 0 \\ A & E_{\rm X} + 2F|\mathcal{P}_0|^2 & 0 & F\mathcal{P}_0^2 \\ 0 & 0 & 2E_{\rm p} - E_{\rm C}^*(\bar{k}) & -\beta^* \\ 0 & -(F\mathcal{P}_0^2)^* & -A^* & 2E_{\rm p} - (E_{\rm X} + 2F|\mathcal{P}_0|^2)^* \end{pmatrix}. \tag{9}$$

The eigenenergies $\Omega(k)$ of the linear problem (equation (8)) characterize the stability of the solution with only one macro-occupied mode. If the sign of the imaginary parts of the eigenenergies $\Omega(k)$ is negative, the solution of equations (5) and (6) with one macro-occupied mode is stable, because the deviations decay exponentially with time, $\propto \exp(\mathrm{Im}\,\Omega(k)t)$, $\mathrm{Im}\,\Omega(k) < 0$. In the opposite case $\mathrm{Im}\,\Omega(k) > 0$, the one-mode solution becomes unstable.

Figure 5 shows the renormalized eigenenergies of the linear problem (8) calculated with $|\mathcal{P}_0|^2 = 0.14$, $|\mathcal{E}_{\rm ext}|^2 = 0.081$, a threshold value for the stimulated scattering into $k_{\rm s} < 0$, $k_{\rm i} > 2k_{\rm p}$. The latter can be understood from the fact that the imaginary part of the eigenenergies (right panel) becomes positive around $k_{\rm s} < 0$, $k_{\rm i} > 2k_{\rm p}$. (There are four eigenenergies of equation (8), but only the pair of them with $\mathrm{Re}\,\Omega(k)$ near the LP branch are physically important and shown in figure 5.)

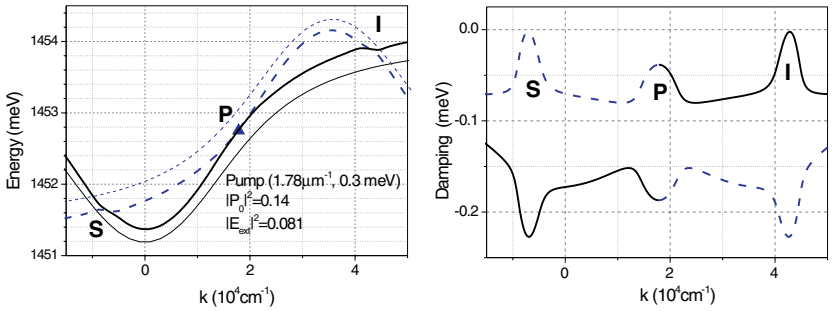


**Figure 5.** Lower polariton branches (left panel) and dampings (right panel), calculated with the pumped exciton polarization $|\mathcal{P}_0|^2 = 0.14$, $|\mathcal{E}_{\rm ext}|^2 = 0.081$. These pump conditions correspond to the threshold of parametric scattering; see the empty circle on the solid curve in figure 4. Simultaneously, these pump conditions are close to the end of the lower stable S-curve branch (the border of the bistability region) of the pumped exciton (see the upward pointing triangle on the solid curve in figure 4). The thick solid (dashed) lines are signal (idler) eigenenergies. The thinner lines in the left panel show the same at low $|\mathcal{P}_0|^2 \approx 0$. The pump is at $k_{\mathbf{p}} = 1.78\ \mu\mathrm{m}^{-1}$ ($\vartheta \approx 14^\circ$) and $\Delta = 0.3$ meV above the unrenormalized LP branch ($\Delta = E_{\rm p} - E_{\rm LP}(\mathbf{k}_0)$). The triangle marks the pump (P) location.

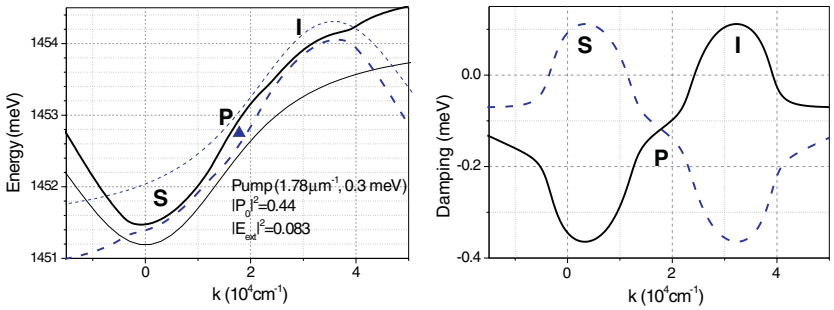


**Figure 6.** Lower polariton branches (left panel) and dampings (right panel), calculated with the pumped exciton polarization $|\mathcal{P}_0|^2 = 0.44$, $|\mathcal{E}_{\rm ext}|^2 = 0.083$. These pump conditions (see the star on the solid curve in figure 4) are realized on the upper S-curve branch after the pumped mode jumps up from the end of the lower stable S-curve branch.

However, at $t \approx 600$ ps, instead of the stimulated scattering into these modes, another instability develops. The trajectory of the system on the $\left[|\mathcal{P}(k_{\rm p}, t)|^2, |\mathcal{E}_{\rm ext}(t)|^2\right]$ plane—see figure 3—shows that the instability at $t \approx 600$ ps is the jump of the $k_{\rm p}$ mode from the lower to the upper branch of the S-shaped curve. Actually, the fact that this instability is approaching can be seen clearly from the existence of the middle maximum (marked by the letter P) in the right panel of figure 5. This maximum grows quickly with $|\mathcal{P}_0|^2$, changing sign (losing stability) at $|\mathcal{P}_0|^2 = 0.16$; compare with figure 7.

In the empty cavity with quadratic dispersion, the upper S′ branch is usually stable [18, 19]. In a MC with inflective LP dispersion, it can become unstable against the parametric scattering. Actually, its stability depends now on the pump position. For the pump in the normal direction, $k_{\rm p} = 0$, i.e., far from the inflection point, it is still stable. As a result, a usual bistability behaviour takes place as demonstrated recently in [24]. In our case, however, the pump is not far from the inflection point, and it brings about a qualitative difference. This can be seen from, e.g., figure 6, showing the signal and idler branches calculated on the upper part of the S-curve at $|\mathcal{P}_0|^2 = 0.44$, $|\mathcal{E}_{\rm ext}|^2 = 0.083$. According to the kinetics of the pumped oscillator

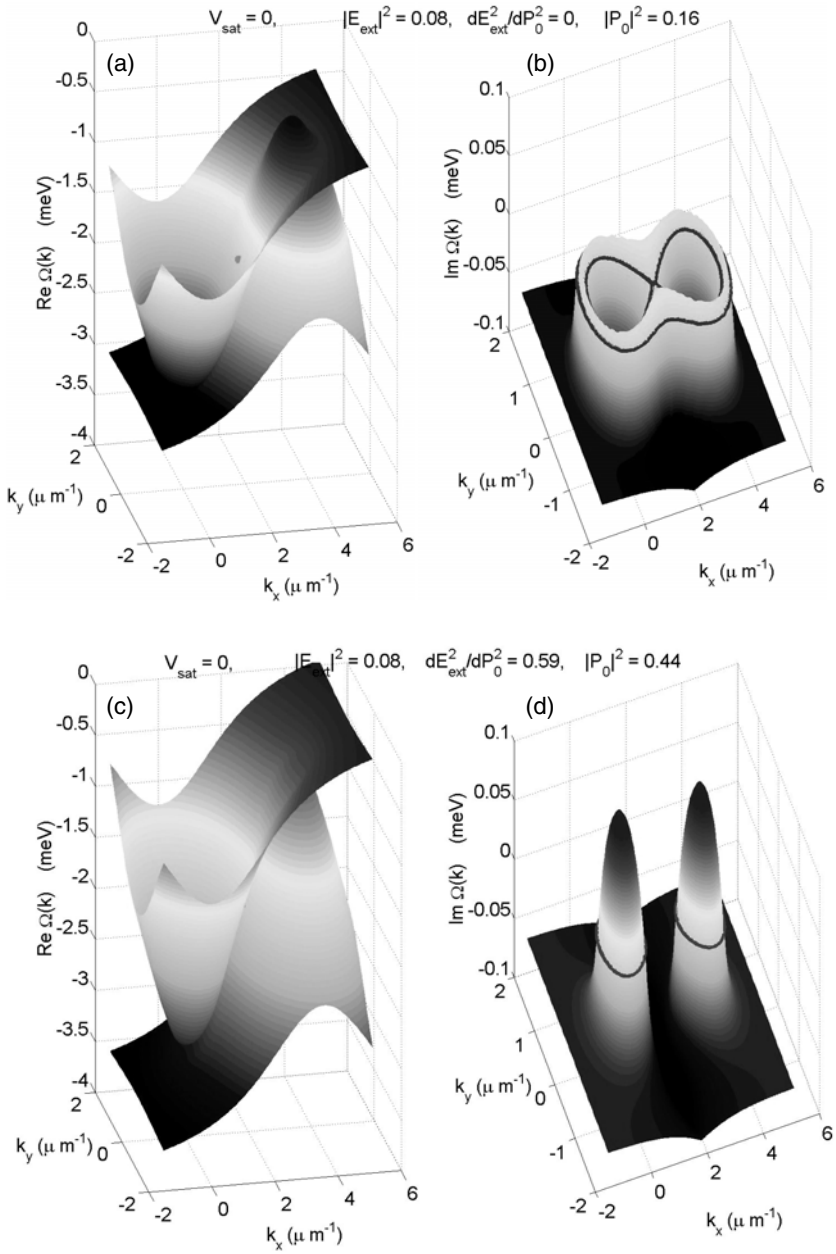


**Figure 7.** The calculated 2D renormalized signal and idler branches in the case of neglecting saturation, $V_{\rm sat} = 0$. Panels (a), (b) show the situation at the end point of the lower branch of the S-curve ($|\mathcal{P}_0|^2 = 0.16$, $\mathcal{E}^2_{\rm ext} = 0.083$), on the right border of the bistability region (see the triangle on the solid S-shaped curve in figure 4). Panels (c), (d) show the situation on the upper branch of the S-shaped curve at $|\mathcal{P}_0|^2 = 0.44$, $\mathcal{E}^2_{\rm ext} = 0.083$ (see the star on the solid S-shaped curve in figure 4). Panels (a), (c) show the functions $\mathrm{Re}\,\Omega(\mathbf{k})$ for both the idler and signal branches. Panels (b), (d) show $\mathrm{Im}\,\Omega(\mathbf{k})$ for the most unstable branches only. Thick solid contours in panels (b), (d) show the stability borders $\mathrm{Im}\,\Omega(\mathbf{k}) = 0$.

in our numerical simulations—see figure 3—it is approximately the place where the pumped oscillator jumps up during the first instability at $t \approx 600$ ps. Instead of damping, a large gain is

realized for polariton modes just with $k_s \approx 0$, $k_i \approx 2k_p$. As a result, a stimulated scattering into these modes develops very quickly (because of a very strong gain). It is fed by the increased pump absorption, as can be understood from the calculation of the MC absorption kinetics.

As a result of developing this instability, the pumped mode eventually jumps back into the lower position (at $t \approx 700$ ps). Now, because we already have a well developed scattered noise in the system, this lower position is more or less stable, although subject to noisy fluctuations because of the already developed scattered states and the competition between them and the pumped mode.

Equation (8) appears to be analogous to that discussed in detail in [9–11]. We use the MC-X basis instead of the UP–LP one. There is an advantage of the MC-X basis: the dependence of the interaction constant $F$ on $k$ can be neglected. Then, in the space representation, it corresponds to a local contact interaction $F \int |\mathcal{P}(x)|^4 \, dx$, which allows a very efficient numerical code for equations (3) and (4) to be written.

## 3. Discussion

As we have shown, the numerical solution of equations (3) and (4) in the one-dimensional approximation and neglecting the exciton saturation can demonstrate sharp thresholds. The analysis of the stability conditions of the solution with only one macro-occupied mode shows that these instabilities are caused by the interplay between the bistable driven nonlinear exciton response and the instabilities due to polariton–polariton parametric scattering.

A question arises of whether these results hold in a full 2D situation, and with accounting for the exciton saturation.

In our 1D numerical calculations, we discretize the continuum of the exciton and photon states into approximately $10^2$ coupled modes. From the numerical point of view, solving of the analogous problem in a full two-dimensional situation can only be done on a supercomputer, because at least $10^4$ coupled modes are needed. We would like to stress here that we solve the full problem of multi-polariton scattering, without *a priori* assumptions on the existence of three occupied modes (as in [7, 9, 10]) or 6–7 occupied modes [11]. It appears that all the scattered exciton and photon states are important for the development of the instabilities discussed.

Let us note firstly that the equation for driven exciton polarization (7) is dimensionality independent. Thus, the S-curve for the driven nonlinear exciton in 2D is actually the same as shown in figure 4. As to the stability equations (8), they are written in a simple analytical form which is valid in the full 2D case too. It is possible to make a full two-dimensional analysis of the stability of the solution with only one macro-occupied mode. Figure 7 illustrates the calculated 2D signal and idler dispersion branches (panels (a), (c)) and damping of the most unstable branch (panels (b), (d)). Panels (a), (b) and (c), (d) illustrate the renormalized spectra calculated for lower and upper positions on the S-curve respectively. (See the triangle and star, respectively, on the solid curve in figure 4, and compare with the 1D spectra in figures 5 and 6, respectively.)

At the lower S-curve branch, slightly below the instability of the pumped oscillator, the parametric scattering instability is already reached—note a thick 8-shaped contour showing the parametric scattering instability borders $\mathrm{Im}\,\Omega(\mathbf{k}) = 0$. At slightly lower pump intensities at the threshold of parametric instability, it transforms into the 8-shaped curve in figure 2 of [9].

As in the 1D case, the solution on the upper branch of the S-curve appears to have a very large gain (strong parametric instability); compare the right panel in figure 6 and panel (d) in figure 7. The regions of strong parametric instabilities can be seen inside the thick round curves on the surfaces $\mathrm{Im}\,\Omega(\mathbf{k})$, showing the condition $\mathrm{Im}\,\Omega(\mathbf{k}) = 0$. The important thing is that the regions of strong parametric instabilities are compact and centred around $\mathbf{k}_s \approx 0$ and

$\mathbf{k}_\mathrm{i} \approx 2\mathbf{k}_\mathrm{p}$ in the 2D as well as in the 1D case. (It is understood that in the 2D case $k_{\mathrm{p},x} = k_\mathrm{p}$ and $k_{\mathrm{p},y} = 0$, as shown in the light scattering scheme in figure 1.) Thus, in the 2D case also, the jump of the pumped mode from the lower to the upper S-curve branch will be accompanied by a fast development of the parametric scattering instabilities into the modes with $k_\mathrm{s} \approx 0$, $k_\mathrm{i} \approx 2k_\mathrm{p}$. This proves the relevance of the scenario discussed for the full 2D case.

We turn now to the influence of the exciton saturation. Strictly speaking, we have to solve the equation for the electron–hole density matrix, coupling the electron–hole populations (diagonal components of the density matrix) with the exciton polarization (off-diagonal). A simplified macroscopic description of the saturation effect can be used, following the approach of [25], when a nonlinear term proportional to $|\mathcal{P}(x)|^2\mathcal{E}(x)$ is added to equation (3) for the polariton polarization. It reads now as

$$\left[\mathrm{i}\frac{\mathrm{d}}{\mathrm{d}t} - E_\mathrm{X}\right]\mathcal{P}(k,t) = A\sum_{q,q'}\left[\delta_{q,k} - V_\mathrm{sat}\mathcal{P}(q',t)\mathcal{P}^*(q+q'-k,t)\right]\mathcal{E}_\mathrm{QW}(q,t) + F\sum_{q,q'}\mathcal{P}(q',t)\mathcal{P}^*(q+q'-k,t)\mathcal{P}(q,t) + \xi(t), \tag{10}$$

where $V_\mathrm{sat}$ is the exciton saturation constant [7, 24]. In the case of GaAlAs microcavities, the dimensionless saturation parameter $V_\mathrm{sat}$ is actually small, $\approx$0.1.[2] This corresponds to the well established fact that such microcavities are ideal systems for investigation of complicated exciton–photon nonlinearities below the exciton saturation.

Equation (7) for the pumped mode itself is modified to

$$(\Delta_\mathrm{PC}\Delta_\mathrm{PX} - \tilde{A}\beta)\mathcal{P}_0 - \Delta_0 F|\mathcal{P}_0|^2\mathcal{P}_0 = \tilde{A}\alpha\mathcal{E}_\mathrm{ext}, \tag{11}$$

that is, via a replacement of $A$ in equation (7) by $\tilde{A} = A\left(1 - V_\mathrm{sat}|\mathcal{P}_0|^2\right)$. The S-shaped curve calculated with $V_\mathrm{sat} = 0.1$ is shown as a dashed line in figure 4.

The effective Hamiltonian matrix equation (9) becomes

$$\begin{pmatrix} E_\mathrm{M}(k) & \beta & 0 & 0 \\ \tilde{A} & E_\mathrm{X} + 2F|\mathcal{P}_0|^2 - AV_\mathrm{sat}\mathcal{P}_0^*\mathcal{E}_0 & 0 & F\mathcal{P}_0^2 - AV_\mathrm{sat}\mathcal{P}_0\mathcal{E}_0 \\ 0 & 0 & 2E_\mathrm{p} - E_\mathrm{M}^*(\bar{k}) & -\beta^* \\ 0 & -(F\mathcal{P}_0^2 - AV_\mathrm{sat}\mathcal{P}_0\mathcal{E}_0)^* & -\tilde{A}^* & 2E_\mathrm{p} - (E_\mathrm{X} + 2F|\mathcal{P}_0|^2 - AV_\mathrm{sat}\mathcal{P}_0^*\mathcal{E}_0)^* \end{pmatrix}.$$

Although, quantitatively, the accounting for the finite exciton saturation $V_\mathrm{sat} = 0.1$ causes changes of all calculated dependences, especially that of the S-curve for the pumped mode (compare the solid and dashed S-curves in figure 4), it does not bring about qualitative differences in the scenario discussed above of the instability development. The latter can be seen, e.g., from the comparison of the calculated renormalized branches with $V_\mathrm{sat} = 0$ and 0.1, shown in figure 8 for the most unstable signal–idler branch only. It can be seen from this comparison that only minor quantitative differences exist between the eigenenergies calculated at the specific points on the S-curves where the sharp transitions of the polariton scattering occur, according to the numerical model. This means that there is a qualitative similarity of the instability developments obtained when we neglect and take into account the saturation effect.

## 4. Conclusions

To summarize, we have demonstrated numerically on a simplified one-dimensional model a strong instability of the polariton–polariton scattering. This instability is a complex interplay between the bistability of the driven nonlinear oscillator and the parametric instabilities of the polariton–polariton scattering. As a result of this instability, the scattered polariton signal is

[2] But not as small as $10^{-2}$ in [24].

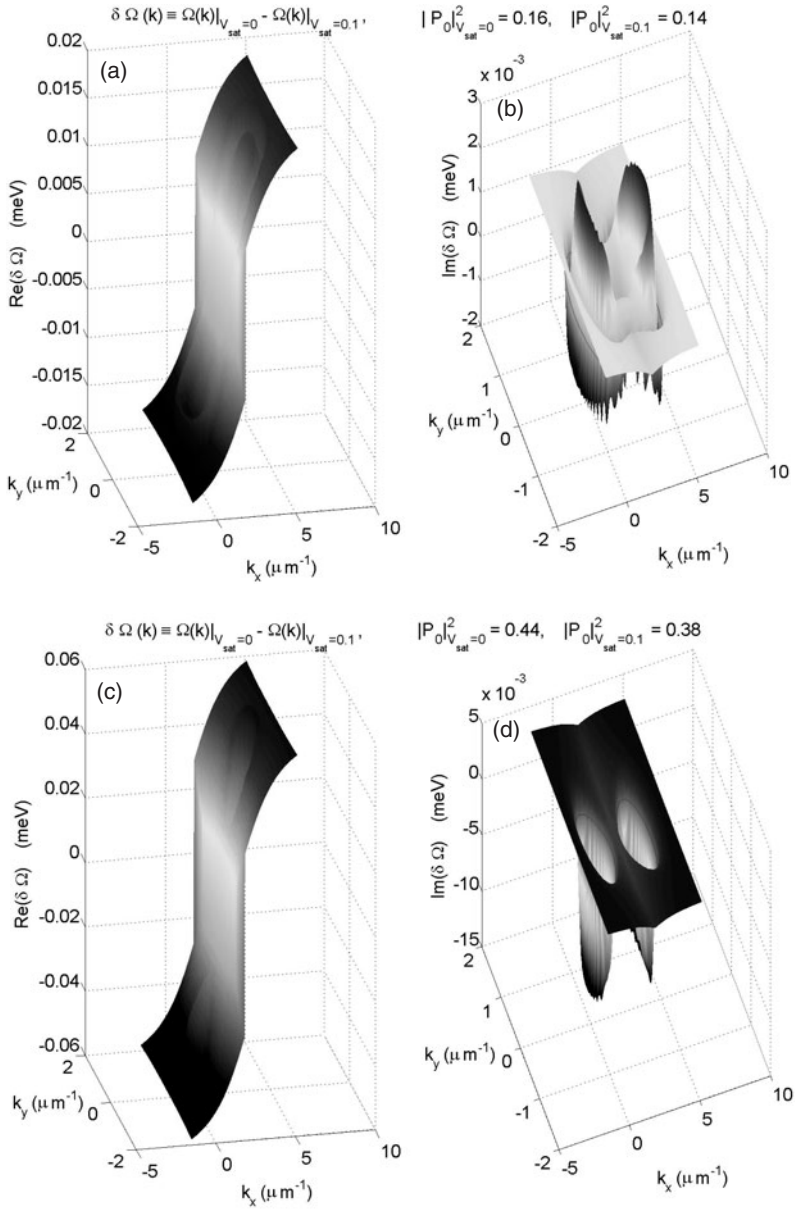


**Figure 8.** The calculated real ((a), (c)) and imaginary ((b), (d)) parts of the difference between the 2D renormalized signal and idler branches neglecting and accounting for the exciton saturation. Panels (a), (b) and (c), (d) show the differences in the end points of the lower branch of the S-curve and on the right border of the bistability region, respectively. In panels (a), (b) the renormalized spectra are calculated with pumped exciton polarization and external field intensity $|\mathcal{P}_0|^2 = 0.16$, $\mathcal{E}^2_{\rm ext} = 0.083$ (for $V_{\rm sat} = 0$) and 0.14, 0.072 (for $V_{\rm sat} = 0.1$), and in panels (c), (d) they are 0.44, 0.083 (for $V_{\rm sat} = 0$) and 0.38, 0.072 (for $V_{\rm sat} = 0.1$); see the triangles and stars on the solid and dashed S-shaped curves in figure 4. Note the much smaller scale of the vertical axes here in comparison with figure 7.

expected to centre around the normal direction $k_{\rm s} \approx 0$. This is in qualitative agreement with the unexpected behaviour of the polariton–polariton scattering under a strong cw excitation

away from the inflection point on the lower polariton branch observed recently [14, 15], when the signal and idler maxima do not shift along the renormalized LP dispersion curve but are always seen at $k_s \approx 0$ and $k_i \approx 2k_p$.

We show that accounting for the two-dimensionality of the polariton–polariton scattering in real MCs as well as of the exciton saturation does not qualitatively change the scenario of instability development discussed.

Finally, we would like to emphasize that the crucial property for the observation of this effect is the inflective form of the LP dispersion in microcavities. Additionally, the pump momentum has to be not too far from the inflection point. In an empty MC, or in a polaritonic MC with the pump near the normal direction, only the bistability effects can be observed.

## Acknowledgments

The authors are grateful to P V Elyutin, L V Keldysh, V D Kulakovskii and M S Skolnick for fruitful discussions. SGT thanks the Organizing Committee of the Photon Mediated Phenomena workshop, Gregynog 2003, for inviting him to this highly informative and well organized meeting. This work was supported in parts by the Russian Foundation for Basic Research, Russian Ministry of Science, Russian Academy of Sciences and INTAS.

## References

[1] Weisbuch C, Nishioka M, Ishikawa A and Arakawa Y 1992 *Phys. Rev. Lett.* **69** 3314
[2] Khitrova G, Gibbs H M, Jahnke F, Kira M and Koch S W 1999 *Rev. Mod. Phys.* **71** 1591
[3] Savvidis P G, Ciuty C, Baumberg J J, Whittaker D M, Skolnick M S and Roberts J S 2000 *Phys. Rev. Lett.* **84** 1547
[4] Houdré R, Weisbuch C, Stanley R P, Oesterle U and Ilegems M 2000 *Phys. Rev. Lett.* **85** 2793
[5] Stevenson R M, Astratov V N, Skolnick M S, Whittaker D M, Emam-Ismail M, Tartakovskii A I, Savvidis P G, Baumberg J J and Roberts J S 2000 *Phys. Rev. Lett.* **85** 3680
[6] Baumberg J J, Savvidis P G, Stevenson R M, Tartakovskii A I, Skolnick M S, Whittaker D M and Roberts J S 2000 *Phys. Rev.* B **62** R16247
[7] Ciuti C, Schwendimann P, Deveaud B and Quattropani A 2000 *Phys. Rev.* B **62** R4825
[8] Tartakovskii A I, Krizhanovskii D N and Kulakovskii V D 2000 *Phys. Rev.* B **62** R13298
[9] Ciuti C, Schwendimann P and Quattropani A 2001 *Phys. Rev.* B **63** 041303
[10] Whittaker D M 2001 *Phys. Rev.* B **63** 193305
[11] Savvidis P G, Ciuty C, Baumberg J J, Whittaker D M, Skolnick M S and Roberts J S 2001 *Phys. Rev.* B **64** 075311
[12] Saba M, Ciuti C, Bloch J, Thierry-Mieg V, Andre R, Dang L S, Kundermann S, Mura A, Bongiovanni G, Staehli J L and Deveaud B 2001 *Nature* **414** 731
[13] Savasta S, Di Stefano O and Girlanda R 2003 *Phys. Rev. Lett.* **90** 096403
[14] Kulakovskii V D, Tartakovskii A I, Krizhanovskii D N, Gippius N A, Skolnick M S and Roberts J S 2001 *Nanotechnology* **12** 475
[15] Butte R, Skolnick M S, Whittaker D M, Bajoni D and Roberts J S 2003 *Phys. Rev.* B **68** 115325
[16] Kulakovskii V D, Krizhanovskii D N, Tartakovskii A I, Gippius N A and Tikhodeev S G 2003 *Usp. Fiz. Nauk* **173** 995
Kulakovskii V D, Krizhanovskii D N, Tartakovskii A I, Gippius N A and Tikhodeev S G 2003 *Phys.—Usp.* **46** 967 (Engl. Transl.)
[17] Gippius N A, Tikhodeev S G, Kulakovskii V D, Krizhanovskii D N and Tartakovskii A I 2004 *Europhys. Lett.* to be published *Preprint* cond-mat/0312214
[18] Firth W J and Scroggie A J 1996 *Phys. Rev. Lett.* **76** 1623
[19] Kuszelewicz R, Ganne I, Sagnes I, Slekys G and Brambilla M 2000 *Phys. Rev. Lett.* **84** 6006
[20] Vladimirov A G, McSloy J M, Skryabin D V and Firth W J 2002 *Phys. Rev.* E **65** 046606
[21] Duffing G 1918 *Erzwungene Schwingungen bei veranderlicher Eigenfrequenz* (Braunschweig: Vieweg)
[22] Luchinsky D G, McClintocky P V E and Dykman M I 1998 *Rep. Prog. Phys.* **61** 889
[23] Gilmore R 1998 *Rev. Mod. Phys.* **70** 1455
[24] Baas A, Karr J Ph, Eleuch H and Giacobino E 2004 *Phys. Rev.* A **69** 023809
[25] Tassone F and Yamamoto Y 1999 *Phys. Rev.* B **59** 10830